Evolution of Acoustic Waves in High-Pressure Compressible Counterflow Diffusion Flames

Geveen Arumapperuma[a], Matthew X. Yao[b], Jean-Pierre Hickey[c], Wang Han[a]

[a]School of Engineering, The University of Edinburgh, Edinburgh EH8 3JL, Scotland, UK
[b]Department of Mechanical and Civil Engineering, The California Institute of Technology, 1200 E. California Blvd. MC 104-44, Pasadena, CA 91125, USA
[c]Department of Mechanical and Mechatronics Engineering, University of Waterloo, Waterloo, ON N2L 3G1, Canada

Abstract

Thermoacoustic instabilities (TAIs) arise due to the coupling between the unsteady heat release rate of the flame and the underlying acoustic field, which can cause excessive mechanical vibrations in combustors, resulting in a reduced lifetime of the combustion engine, or in extreme cases can lead to catastrophic failure of the system. Therefore, understanding the evolution of acoustic waves in flames is fundamental to mitigating the serious side effects of TAIs. While flame-acoustic interaction has been studied extensively in premixed flames, little effort has been made to explore the evolution of acoustic waves in diffusion flames. This study aims to numerically investigate acoustics in a hydrogen-air counterflow diffusion flame at high pressure conditions. To this end, a fully compressible unsteady reacting flow solver is employed to simulate the flame under a temporally and spatially evolving pressure field. Under the assumption of fully reflecting boundary conditions, for all tested pressures (1-60 bar) a growth in the acoustics can be observed, where the acoustic pressure perturbations grow with time indicating a coupling between the heat release rate and the acoustic field. The growth rate of the acoustics is found to be significantly larger at 5 bar than at 1 bar. However, above 5 bar, the growth rate saturates, where the growth rate of the acoustics marginally increase with pressure. Spectral analysis showed the pressure perturbations on the low-density fuel side to be more periodic compared to the high-density oxidizer side. The periodicity is found to reduce as the pressure increased where more complex acoustics with multiple frequencies start to develop.

1 Introduction

Thermoacoustic instability (TAI) is a phenomenon first studied by Lord Rayleigh in 1878 [1]. As explained in [1], TAIs arise from the interaction between the unsteady heat release of the flame and the underlying acoustic field. The imperfect burning of the flame will result in an unsteady heat release causing the flame to oscillate. This will generate acoustic waves within the combustion chamber which will reflect off the combustor walls and return to influence their own source. If the reflected acoustic waves couple with the unsteady heat release rate of the flame, the acoustics will amplify resulting in large amplitude oscillations known as self-sustaining thermoacoustics. These oscillations will cause excessive mechanical vibrations in the system which will reduce the lifetime of the combustor, increase

Correspondence to: wang.han@ed.ac.uk

the heat transfer to the combustor walls degrading the performance of the combustor, and in extreme cases can cause catastrophic failure of the system [2]. Therefore, understanding the behaviour of TAIs is fundamental to mitigating the serious side effects of TAIs.

Studies regarding TAIs in premixed flames are of abundance. However, the investigation of TAIs in diffusion flames is very rare. Diffusion flames are widely used in many practical applications for two main reasons: (a) non-premixed burners are easier to design and build, as perfect mixing of reactants in specific proportions is not needed; and (b) diffusion flames are safer to operate as the fuel and oxidizer are injected separately and hence the flame cannot back-propagate or auto-ignite in undesired locations [3]. This motivates us to investigates TAIs in diffusion flames in this work.

Due to the high computational expense of simulating three-dimensional diffusion flames with detailed chemistry especially at high-pressure conditions, a transient **c**ounterflow **d**iffusion **f**lame configuration is widely used to explore the fundamental unsteady dynamics of diffusion flames, which is also employed in this work. The majority of the previous studies on the unsteady counterflow diffusion flame have been focused on the hydrodynamic effects on the flame (i.e., velocity and strain rate fluctuations) [4–9], and only a few studies have been conducted about thermodynamic effects (i.e., flame response to acoustic pressure fluctuations) [10–13] which are responsible for thermoacoustic instabilities. These studies have some limitations which are summarized below. [4–9] made the isobaric assumption where the pressure is assumed to be constant. These studies mainly investigated the response of counterflow flames to a fluctuating inlet velocity or strain rate. Flame-acoustic interactions are not studied. On the other hand, [11–13] made the low Mach number assumption where the acoustic wavelengths are assumed to be much larger than the computational domain, such that the acoustic fluctuations are approximately uniform throughout the domain and pressure is only a function of time. In this context, acoustic propagation through the domain can not be captured, and the analysis is only limited to low frequency acoustics.

The above review indicates that the previous work about unsteady dynamics of CDFs was conducted in the context of low-Mach number or incompressible flows which are not suitable for studying TAIs of CDFs. In this sense, the flame-acoustic interaction in CDFs is still not well understood. Recently, Yao [14] numerically investigated a fully compressible H_2-air CDF, with special attention on the behaviour of self-sustaining thermoacoustics under different strain rates (300 s^{-1} and 5000 s^{-1}). More recently, Yao et al [15] investigated the response of a H_2-air flame under external oscillations. Sinusoidally varying pressure field was introduced at the fuel inlet for a range of frequencies (1-4000 kHz) and the response of the flame was studied. Zambon and Chelliah [16] investigated the behaviour of self-sustaining TAIs of CH_4-air counterflow flames and showed the importance of using detailed chemistry in accurately predicting thermoacoustics.

One limitation of these studies [14–16] is that all numerical simulations were conducted at a normal pressure (1 bar) unrealistic in real-world applications. With this background, this study aims to understand the behaviour of self-sustaining TAIs in CDFs without any of the aforementioned limitations. To this end, a series of fully compressible H_2-air unsteady CDFs with detailed chemistry is numerically studied with pressures ranging from 1-60 bars.

2 Methodology

2.1 Governing equations of compressible CDF

The following unsteady fully compressible governing equations for describing compressible CDFs, which were derived by Zambon and Chelliah [16], are employed in this study.

$$\frac{\partial \rho}{\partial t} + \frac{\partial \rho u}{\partial x} + 2\rho V = 0, \tag{1}$$

$$\frac{\partial \rho Y_k}{\partial t} + \frac{\partial \rho u Y_k}{\partial x} + \frac{\partial \rho V_k Y_k}{\partial x} + 2\rho Y_k V = \dot{\omega}_k, \tag{2}$$

$$\frac{\partial \rho u}{\partial t} + \frac{\partial \rho u u}{\partial x} + \frac{\partial p_0}{\partial x} + 2\rho u V = \frac{\partial}{\partial x}\left[\frac{4}{3}\mu\left(\frac{\partial u}{\partial x} - V\right)\right] + 2\mu\frac{\partial V}{\partial x}, \tag{3}$$

$$\frac{\partial \rho V}{\partial t} + \frac{\partial \rho u V}{\partial x} + 3\rho V^2 = -2p_2 + \frac{\partial}{\partial x}\left[\mu\frac{\partial V}{\partial x}\right], \tag{4}$$

$$\begin{aligned}\frac{\partial \rho h_t}{\partial t} - \frac{\partial p_0}{\partial t} + \frac{\partial \rho u h_t}{\partial x} + 2\rho h_t V = \frac{\partial}{\partial x}\left[\lambda\frac{\partial T}{\partial x}\right] - \sum_{k=1}^{n_s}\frac{\partial \rho Y_k V_k h_k}{\partial x} \\ + \frac{\partial}{\partial x}\left[\frac{4}{3}\mu\left(\frac{\partial u}{\partial x} - V\right)u\right] + 2\mu\frac{\partial V}{\partial x}u - \frac{4}{3}\mu\left(\frac{\partial u}{\partial x} - V\right)V\end{aligned} \tag{5}$$

where $\dot{\omega}_k$ represents the species mass production rate for the k^{th} species, μ the dynamic viscosity, λ the thermal conductivity, h_k the sensible enthalpy for the k^{th} species, h_t the total enthalpy of the system, P_0 the axial pressure, P_2 the radial pressure gradient, V the radial velocity, u the axial velocity, and T the temperature. The term $\rho Y_k V_k$ represents the diffusive flux for the k^{th} species where V_k is the diffusion velocity. The diffusive flux calculates the molecular diffusion between chemical species and is calculated using the mixture averaged diffusion model [17]. To solve the governing equations, it is required to define a relationship between pressure, temperature and density through an equation of state (EoS). In this study, the Peng-Robinson [18] EoS is used to consider real-gas effects. It is worth mentioning that equations 2-5 are derived without any major ideal gas assumptions. Thus it is applicable with the Peng-Robinson Eos. A detailed chemistry [19] for H_2-air is considered, containing 9 chemical species and 27 reactions, which has been extensively validated in high-pressure conditions.

2.2 Numerical method

A novel one-dimensional finite volume code, OneD Thermocode [14, 15], is employed to solve the above equations. The solver is coupled with Cantera [20] which is used to calculate transport and thermodynamic properties. Furthermore, the Peng-Robinson EoS is implemented in the numerical framework to consider real gas effects at high pressures. The solver calculates the fluxes at the cell surfaces using a flux reconstruction method [21] with polynomial interpolation to determine the flux at the cell wall. Two polynomials are fitted through three cell centres, one with two cell centres to the left of the cell wall, and the other to the right. The values obtained from the left and right biased fluxes are then averaged at the cell wall to obtain an approximate value at the location. For more details about this approach, the reader is referred to [14]. It is noted that time-dependent Navier-Stokes Characteristic Boundary Condition (NSCBC) [22] is employed to capture acoustic reflections at the boundaries.

2.3 Operating conditions

The CDF can be described as a strained flame as the oxidizer and fuel streams are strained against each other. The rate of the straining can be quantified by the strain rate and is typically used to characterise the flame as it affects the overall structure of the flame. In this paper, the global strain rate a is defined as the average velocity gradient across the computational domain:

$$a = \frac{|u(x = L) - u(x = 0)|}{L} \tag{6}$$

where L is the length of the computational domain (i.e., separation distance between fuel and oxidizer inlets) and u is the velocity.

The solver requires an initial solution to initialize and solve the unsteady governing equations. The initial solution is provided by solving the steady-state governing equations using Cantera. As the focus of this study is to investigate the effects of pressure on the thermoacoustics, the strain rate for all simulations are kept constant at $a = 1000\,\mathrm{s}^{-1}$. The operating conditions are summarized in table 1 below. The H_2-air CDF consists of a fuel stream of pure H_2 and an oxidizer stream of $0.21\,O_2$ and $0.79\,N_2$ by mole fraction. A domain size of 0.004m is used for pressures above 5 bar while a larger domain size of 0.02m is used at 1 bar. This is because at low pressure the flame thickness is much larger than at high pressure and hence a larger domain size has to be used.

Table 1: Operating conditions considered in this work

Pressure (bar)	Fuel inlet temperature (K)	Oxidizer inlet temperature (K)	Fuel mass flow rate (kg $m^{-2}s^{-1}$)	Oxidizer mass flow rate (kg $m^{-2}s^{-1}$)	Grid spacing (μm)
1	298	298	1.29	4.88	20
5	298	298	1.28	4.88	20
10	298	298	2.56	9.76	10
20	298	298	5.10	19.50	6.67
40	298	298	10.10	38.90	3.33
60	298	298	14.98	58.13	2.86

3 Results and discussion

3.1 Pressure and real-gas effects on flame structure

In this section, the steady CDFs are simulated to investigate the effects of pressure and real gas on the flame structure. Figure 1a shows that the maximum flame temperature significantly increases with pressure. Moreover, this increase in temperature is very non-linear. The comparison between Peng-Robinson EoS and ideal gas EoS indicates that a slight deviation in flame temperature between ideal and real gases starts to develop when $P > 30\,\mathrm{bar}$. At the maximum pressure tested, $P = 100\,\mathrm{bar}$, the difference in flame temperature is about 19 K.

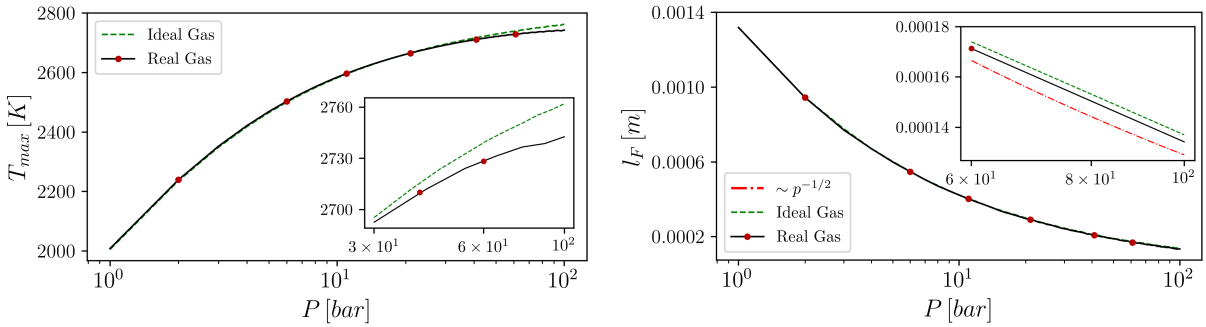

(a) Maximum Temperature

(b) Flame Thickness

Figure 1: Shows the relationship between pressure, maximum flame temperature and thickness. The markers indicate the pressures at which thermoacoustic instabilities are studied.

Figure 1b shows that the flame thickness considerably reduces with pressure. Moreover, Fig. 1b illustrates that the real gas effects on the flame thickness is negligible. It is noted that previous studies [15, 23] have shown that the flame thickness is inversely proportional to the square root of pressure times strain rate, $l_F \sim 1/\sqrt{pa}$. Since in this study, the strain rate is constant, flame thickness is only a function of pressure. The numerical results closely correlate with this relationship as shown in figure 1b. Note that this curve is offset from the numerical results for clarity. If an empirical constant of 0.00131 is used such that $l_F = 0.00131 \times 1/\sqrt{p}$, a one-to-one correlation with the numerical results can be obtained. The above analysis indicates that pressure has a significant impact on flame dynamics and that the effects of real gas are negligible at the high-pressure conditions considered in this work.

3.2 Evolution of Acoustic Waves

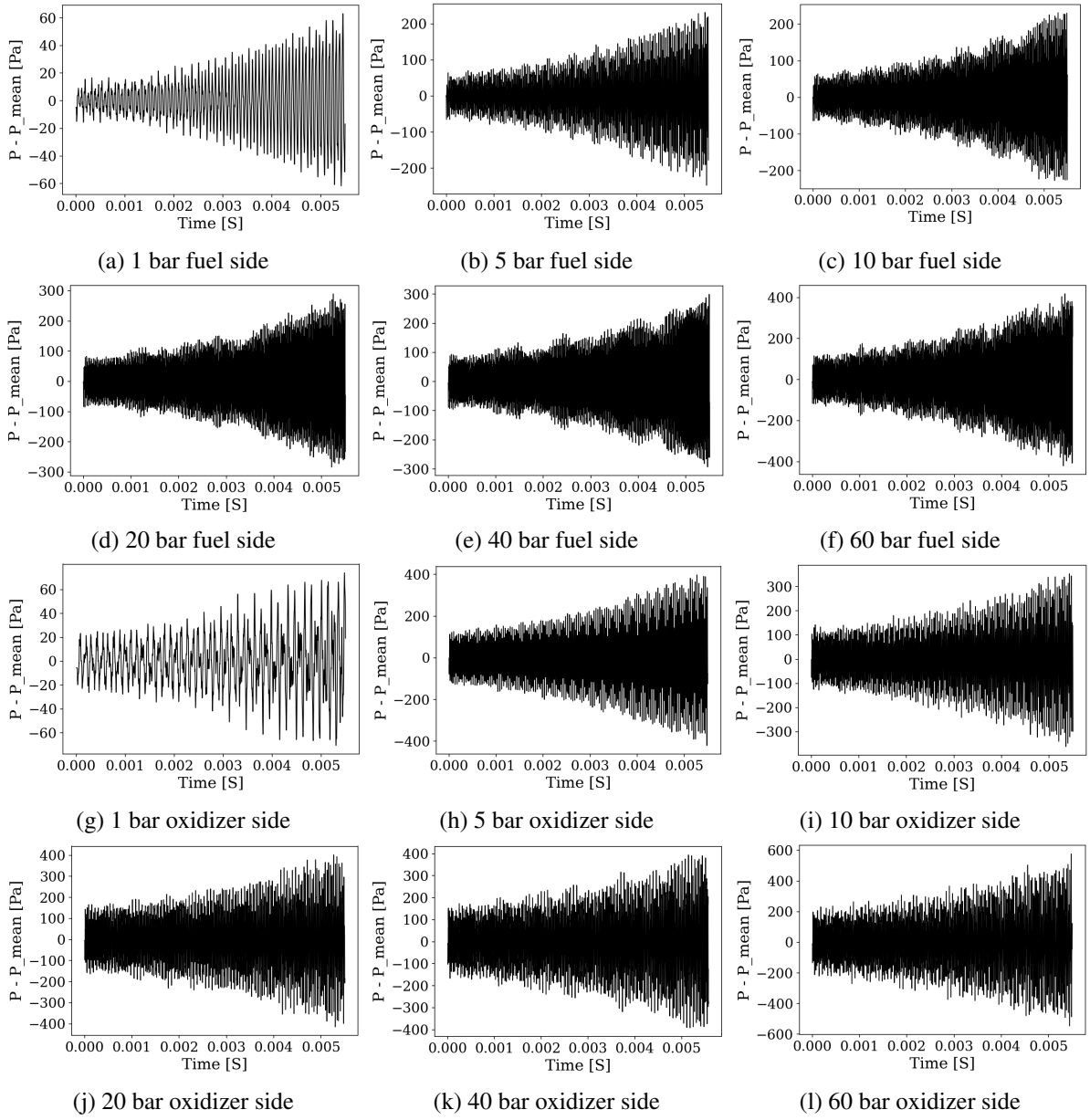

(a) 1 bar fuel side (b) 5 bar fuel side (c) 10 bar fuel side

(d) 20 bar fuel side (e) 40 bar fuel side (f) 60 bar fuel side

(g) 1 bar oxidizer side (h) 5 bar oxidizer side (i) 10 bar oxidizer side

(j) 20 bar oxidizer side (k) 40 bar oxidizer side (l) 60 bar oxidizer side

Figure 2: Acoustic growth on the fuel and oxidizer streams.

The steady-state solution is used to initialise and run the unsteady solver under fully reflecting boundaries, where the acoustic waves are reflected off the boundaries without any damping. To study the stability of the system, initial instability needs to be present in the system. Since the governing equations and the numerical schemes used to generate the initial solutions (i.e., Cantera) are different to that of the unsteady solver (i.e., OneD Thermocode), initial acoustic perturbations are automatically introduced to the solution as the solution fully adjusts to the unsteady governing equations. Therefore, no external perturbations are introduced to the solution. The initial acoustic perturbations are allowed to reflect off the boundaries and interact with the flame, while the pressure in the system is measured at two points along the computational domain. If the domain size is L, for consistency the pressure is always measured at $1/4\,L$, fuel side, and $3/4\,L$, oxidizer side. Since there is a large difference in density between the fuel and oxidizer streams, it will influence the behaviour of the acoustics. Therefore, it is important to measure the acoustics on both sides. The results for the evolution of the initial acoustic perturbations at different pressures are shown in Fig. 2.

It is seen that TAIs present at all tested pressures where the acoustics in the system amplifies with time. There is a large difference in the acoustic growth rate between 1 bar and 5 bar. According to Rayleigh's criterion, the driving force of the instability arises due to the coupling between the heat release rate fluctuations of the flame and the acoustics. Since an increase in pressure intensifies the burning rate of the flame and thus an increase in heat release rate. The coupling between this high energy heat release rate fluctuations and the initial acoustic perturbations could result in high energy acoustics in the system, in the form of large amplitude and high frequency pressure perturbations. Yao [14] conducted a similar study where instead of changing the pressure, the strain rate was changed. Their results show that the acoustic growth is heavily dependent on the strain rate, where increasing strain rates increased the acoustic growth. A similar effect can be observed in this study by increasing the pressure while the strain rate is constant, showing that the acoustic growth is also pressure dependent.

Unlike the large difference in growth rate observed between 1 bar and 5 bar, the increase in growth rate above 5 bar is minor. However, the largest growth rate can be observed at 60 bar where the maximum acoustic amplitude is around 420 Pa on the fuel side, and around 550 Pa on the oxidizer side at time $t = 0.0055\,s$, as shown in Figs. 2f and 2l, respectively. This growth rate saturation at higher pressures can be explained by considering how acoustic waves travel through a medium. Acoustic waves travel through a medium by vibrating its molecules. These vibrations will cause a loss of acoustic energy as heat. The larger the amplitude of sound, the larger the acoustic losses. Furthermore, as the density of the medium increases with the increase in pressure, the number of molecules per unit volume increases, therefore, more molecules will vibrate as the acoustics propagate, increasing the acoustic losses in the system. Therefore, acoustic losses are higher at increasing pressures. However, the driving force of the acoustics increase with pressure, which approximately balances with the increase in acoustic losses, therefore, the growth rate of the acoustics has little change at higher pressures (i.e., above 5 bar) as shown in figure 2.

To study the behaviour of the acoustics further, the frequencies of the perturbations in the low and high-density sides are extracted through a spectral density analysis. The Lomb-Scargle periodogram is employed to extract the dominant frequencies, as it is more suited to analyse uneven data series. The dominant frequencies were extracted from the spectral analysis and are presented in table 2.

The results show that thermoacoustics at the low density fuel side have a single dominant frequency indicating periodic perturbations. However, a second higher frequency starts to develop at 60 bar, indicating that perturbations are becoming less periodic at higher pressures. The high density oxidizer side contains multiple frequencies at all tested pressures. This means that the pressure perturbations at the high-density side are less periodic compared to the low-density side. To understand the multiple frequencies extracted, the pressure field needs to be examined further. The fully reflecting boundary

Table 2: Shows the perturbation frequencies obtained from the spectral analysis

Pressure (bar)	Frequency, fuel stream (kHz)	Frequency, oxidizer stream (kHz)
1	14.62	8.94, 14.62
5	73.65	47.32, 73.65
10	73.21	45.69, 73.21
20	73.36	44.38, 73.36
40	74.08	43.48, 74.08, 103.06
60	74.88, 102.61	43.39, 74.88, 102.61

condition produces a standing wave pressure oscillation between the left and right-hand boundaries. The frequency of these standing waves corresponds to the frequency found in both the fuel and oxidizer streams. For example, at 10 bar of pressure the frequency of 73.21 kHz is found on both reactant streams indicating the standing wave frequency. Note that for 1 bar of pressure the standing wave frequency is much lower than the rest of the results. This is because the domain size used for the 1 bar simulation was much bigger than the rest of the simulations, this increase in domain size has reduced the values of the dominant frequencies while the growth rate of the acoustics is unaffected.

There is a large difference in density between H_2 and air, H_2 being a light species has a much lower density compared to air. This causes a large density gradient to form near the stagnation plane where H_2 and air is mixed. This density gradient increases as the pressure increase. Due to this large difference in density, part of the acoustic wave arriving at this density gradient will be reflected. This reflection produces travelling waves across the flame, a phenomenon that was also observed by Yao [14]. These travelling waves are shown in figure 3a and they propagate at a much higher frequency compared to the standing wave frequency, explaining the higher frequencies (102.61 - 103.06 kHz). However, the degree of reflection seems to be higher when the acoustics travel from the high-density oxidizer side to the low-density fuel side. Therefore, the formation of travelling waves are much stronger on the oxidizer side, as shown in Fig. 3a. However, when the density gradient between the fuel and oxidizer becomes large enough (i.e., at higher pressures), the reflection of the acoustics become large enough to produce substantial travelling waves on the low-density fuel side giving rise to the high frequencies observed on the fuel stream at 60 bar of pressure.

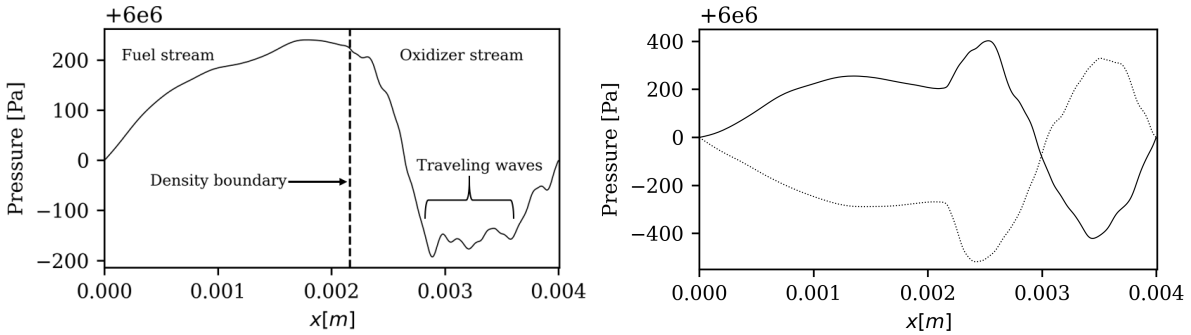

(a) Traveling waves

(b) Standing waves

Figure 3: (a) The travelling acoustic wave propagating in the oxidizer stream at 60 bar; (b) The pressure field at two points showing the formation of the second standing wave on the oxidizer side at 60 bar.

Apart from the high frequencies extracted, low frequency perturbations (8.94 - 45.69 kHz) are also observed on the oxidizer stream. The high degree of acoustic reflectivity at the density boundary on the

oxidizer side, almost acts as a third boundary and will lead to the formation of another standing pressure wave between the density gradient and the right-hand side boundary, as shown in Fig. 3b. The oscillation of this standing wave relative to the standing wave between the left and right-hand side boundaries will give rise to the low frequency perturbations. Since the second standing wave only forms on the oxidizer side, the low frequencies are not found on the fuel side. This second standing wave is also the reason the acoustic amplitudes on the oxidizer stream is higher than in the fuel stream, as shown in Fig. 2

4 Conclusion

In this work, the evolution of acoustic waves in high-pressure diffusion flames is numerically investigated by simulating a fully compressible hydrogen-air counterflow diffusion flame. The Navier-Stokes Characteristic Boundary conditions (NSCBC) are employed to account for the fully reflecting boundary conditions. Under the assumption of fully reflecting boundaries, self-sustaining thermoacoustics are investigated at different pressures ranging from 1-60 bar at a constant strain rate of $1000\,\mathrm{s}^{-1}$. All tested cases showed acoustic growth with time, where the acoustic growth is found to be much faster at 5 bar compared to that at 1 bar. However, the growth rate of the acoustics gets saturated above 5 bar. This is because the high-density environment at elevated pressures increase the acoustic impedance, resulting in a larger energy loss and hence limiting the acoustic growth rate.

Moreover, the frequencies of the acoustic perturbations are extracted using the Lomb-Scargle periodogram. The frequency analysis shows multiple frequencies presented in the acoustic perturbations. Due to the large density gradient across the fuel and oxidizer streams, the acoustic waves tend to reflect off this density boundary producing high frequency travelling waves across the reactant streams. It was found that the reflectivity of the density boundary is higher on the oxidizer side. The reflectivity on the fuel side became large enough to generate travelling waves only at higher pressures (at 60 bar). Furthermore, a standing wave is found to form between the fuel and oxidizer boundaries, typical for fully reflecting boundaries, as confirmed by previous research. However, at high pressures a second standing wave can be formed, resulting in an additional frequency mode presented on the oxidizer side.

References

[1] J. Rayleigh, The Explanation of Certain Acoustical Phenomena, Nature 18 (455) (1878) 319–321.

[2] S. Candel M, Combustion instabilities coupled by pressure waves and their active control, Symposium (International) on Combustion 24 (1) (1992) 1277–1296.

[3] T. Poinsot, D. Veynante, Theoretical and Numerical Combustion, 2nd Edition, R.T Edwards Inc, 2005.

[4] F. N. Egolfopoulos, C. S. Campbell, Unsteady counterflowing strained diffusion flames: diffusion-limited frequency response, Journal of Fluid Mechanics 318 (1996) 1–29.

[5] F. N. Egolfopoulos, Structure and extinction of unsteady, counterflowing, strained, non-premixed flames, International Journal of Energy Research 24 (11) (2000) 989–1010.

[6] H. Lm, C. Law, J. Kim, F. Williams, Response of counterflow diffusion flames to oscillating strain rates, Combustion and Flame 100 (1-2) (1995) 21–30.

[7] T. Saitoh, Y. Otsuka, Unsteady Behavior of Diffusion Flames and Premixed Flames for Counter Flow Geometry, Combustion Science and Technology 12 (4-6) (1976) 135–146.

[8] A. Cuoci, A. Frassoldati, T. Faravelli, E. Ranzi, Frequency Response of Counterflow Diffusion Flames to Strain Rate Harmonic Oscillations, Combustion Science and Technology 180 (5) (2008) 767–784.

[9] A. Cuoci, A. Frassoldati, T. Faravelli, E. Ranzi, Formation of soot and nitrogen oxides in unsteady counterflow diffusion flames, Combustion and Flame 156 (10) (2009) 2010–2022.

[10] C. Sohn, S. Chung, S. Lee, J. Kim, Structure and acoustic-pressure response of hydrogen-oxygen diffusion flames at high pressure, Combustion and Flame 115 (3) (1998) 299–312.

[11] C. Sohn, S. Chung, Effect of pressure on the extinction,acoustic pressure response and NO formations in diluted hydrogen-air diffusion flames, Combustion and Flame 121 (1-2) (2000) 288–300.

[12] C. Sohn, Unsteady analysis of acoustic pressure response in N2 diluted H2 and air diffusion flames, Combustion and Flame 128 (1-2) (2002) 111–120.

[13] A. D. Weiss, F. A. Williams, The acoustic response of Burke-Schumann counterflow flames, Combustion and Flame 192 (2018) 25–34.

[14] M. X. Yao, Thermoacoustic Instabilities in Counterflow Diffusion Flames, Master's thesis, University of Waterloo, Ontario, Canada (2019).

[15] M. X. Yao, J.-P. Hickey, G. Blanquart, Thermoacoustic response of fully compressible counterflow diffusion flames to acoustic perturbations (Article in preparation), Combustion and Flame (2021).

[16] A. Zambon, H. Chelliah, Self-sustained acoustic wave interractions with counterflow flames, Journal of fluid mechanics 560 (2006) 249–278.

[17] J. O. Hirschfelder, C. F. Curtiss, R. B. Bird, M. G. Mayer, Molecular theory of gases and liquids, Wiley, New York, 1964.

[18] D. B. Robinson, D.-Y. Peng, S. Y.-K. Chung, The developing of the Peng-Robinson equation and its application to phase equilibrium in a system containing methanol, Fluid Phase Equilibria 24 (1-2) (1985) 25–41.

[19] M. P. Burke, M. Chaos, Y. Ju, F. Dryer, S. J. Klippenstein, Comprehensive H2/O2 kinetic model for high-pressure combustion, International Journal of Chemical Kinetics 44 (7) (2012) 444–474.

[20] D. Goodwin, H. Moffat, R. Peth, Cantera: An Object-oriented Software Toolkit for Chemical Kinetics, Thermodynamics, and Transport Processes. (2015).

[21] H. T. Huynh, A flux reconstruction approach to high-order schemes including discontinuous Galerkin methods, in: 18th AIAA Computational fluid dynamics conference, Miami, FL, 2007.

[22] T. Poinsot, S. Lelef, Boundary conditions for direct simulations of compressible viscous flows, Journal of Computational Physics 101 (1) (1992) 104–129.

[23] A. J. Juanos, W. A. Sirignano, Pressure effects on real-gas laminar counterflow, Combustion and Flame 181 (2017) 57–70.